Lab on a Chip

PAPER

Published on 31 July 2026
Licence and permissions

Check for updates

Cite this: DOI: 10.1039/d6lc00214e

An injection-molded focal filter-integrated AI platform for cost-effective and highly sensitive molecular point-of-care testing

Tao Zhang,†[ab] Feibiao Pang,†[c] Yao Chen,†[b] Yinghao Du,†[bd] Chengen Song†[b] and Jinzhao Song *[abd]

The growing global demand for precise and accessible diagnostics underscores the need for decentralized, laboratory-grade molecular testing solutions. Current platforms are hindered by the high cost and fragility of glass optical filters with inorganic thin-film coatings, as well as operational complexity that limits deployment in community and home settings. To overcome these barriers, we developed the WeD-1 Pro, a 290 g molecular point-of-care testing (POCT) system designed for both human and veterinary diagnostics. Through systematic screening of polymer substrates and organic optical filter pigments, tailored phthalocyanine blue exhibited superior 480 nm excitation blocking and optimal 525 nm transmission when incorporated into polycarbonate (PC), making it suitable for injection-molded filter fabrication. Using this optimized formulation, a focal filter was produced *via* single-step injection molding. By integrating this newly developed focal filter, the platform achieves low-cost, high-performance fluorescence detection. The platform further incorporates an AI-powered assistant and multi-terminal connectivity, providing rapid, cost-effective, and highly sensitive diagnostics suitable for home and primary care use. In a proof-of-concept demonstration of at-home self-testing, when combined with a one-tube/one-step LAMP–CRISPR panel (LOD: 100 copies per reaction) targeting nine common respiratory pathogens, the system achieved 100% concordance with commercial qPCR assays for SARS-CoV-2 and influenza using self-collected at-home swab samples. For veterinary applications, the WeD-1 Pro was deployed in 40 small veterinary clinics across China's Greater Bay Area between December 2024 and September 2025, where it enabled 1000 on-site 7-plex feline respiratory pathogen tests under routine clinical conditions. Overall, 87% of samples were positive for at least one pathogen. A representative subset of 60 clinical samples was further validated against reference PCR, demonstrating 98% concordance. By integrating advanced diagnostic performance with affordability and accessibility, the WeD-1 Pro offers a transformative solution for primary care, home-based healthcare, and future large-scale epidemiological surveillance.

Received 6th March 2026,
Accepted 28th July 2026

DOI: 10.1039/d6lc00214e

rsc.li/loc

1. Introduction

Frequent outbreaks of infectious diseases, coupled with the growing demand for an improved quality of life, have fueled the need for accurate, user-friendly, cost-effective, and highly sensitive at-home testing solutions.[1] This expanding interest in personal health monitoring extends beyond individual well-being to encompass areas such as food safety, pet care, genetically modified organisms, and meat authenticity.[2] At the same time, primary care settings—including primary care physician (PCP) offices, rural health clinics (RHCs), retail health clinics, and community health centers—face a similar demand for diagnostic solutions that are rapid, accurate, simple to use, affordable, and highly sensitive.[3]

Molecular point-of-care testing (POCT) holds great promise in meeting the growing demand for rapid, accessible diagnostics.[4] Unlike conventional laboratory-based methods, molecular POCT systems are designed to operate in non-professional environments such as homes and primary care settings, requiring devices that are both portable and cost-effective.[2,5–7] Fluorescence-based molecular POCT platforms generally achieve higher analytical sensitivity and specificity than colorimetric systems. However, despite their advantages

[a] *Academy of Medical Engineering and Translational Medicine, Medical College, Tianjin University, Tianjin, 300072, China*
[b] *Hangzhou Institute of Medicine, Chinese Academy of Sciences, Zhejiang Cancer Hospital, Hangzhou, Zhejiang 310022, China*
[c] *Hangzhou EzDx Technology Co., Ltd., Hangzhou, Zhejiang 311231, China*
[d] *School of Molecular Medicine, Hangzhou Institute for Advanced Study, University of the Chinese Academy of Sciences, Hangzhou, Zhejiang 310024, China.*
E-mail: songjinzhao@ucas.ac.cn
† The first five authors contributed equally.

in enabling rapid, on-site molecular analysis, the widespread adoption of fluorescence POCT devices is still constrained by high costs and complex system designs. A major challenge lies in achieving highly sensitive fluorescence detection, which is critical for accurate diagnostics. Current molecular POCT devices typically rely on glass-based optical filters with specialized coatings for fluorescence filtering. These glass filters are expensive, difficult to manufacture, and lack plasticity, limiting their suitability for multifunctional or low-cost device designs.[8,9] Additionally, fluorescence signal focusing in these systems is often achieved using glass convex lenses, further increasing costs and adding bulk to the fluorescence read-out module. While glass filters and convex lenses perform well in microscopy and spectroscopy, their high cost and manufacturing complexity hinder integration into affordable POCT platforms.

Although molecular POCT systems have made significant progress in affordability and usability, they still fall short of fully meeting the needs of both home users and primary care settings. For at-home testing, individuals often lack sufficient knowledge to interpret results and take appropriate follow-up actions, such as therapy planning, or medication access.[10,11] For primary care usage, essential functions such as seamless patient data integration, automatic report generation for physicians, and effective data management for broader epidemic research remain limited. Furthermore, while mobile apps can support at-home users, web-based applications are often more practical for primary care—but current systems do not adequately address this requirement.[12,13] As a result, existing molecular POCT platforms have yet to deliver a comprehensive solution that fully satisfies the practical demands of both home and primary care testing environments.[14,15]

Recent advances in artificial intelligence (AI), particularly machine learning-based data analysis and field-deployable analytical systems, have demonstrated significant potential to enhance POCT performance.[16] AI-assisted signal processing, pattern recognition, and predictive modeling have been successfully applied to improve sensitivity, specificity, and robustness in biosensing platforms.[5,17,18] Moreover, the integration of mobile terminals with portable diagnostic devices enables automated result uploading,[19–21] thereby supporting intelligent algorithm-based real-time result interpretation. Together, these developments highlight the growing role of AI in advancing POCT toward more accurate, scalable, and data-connected diagnostic ecosystems.

To address these challenges, we developed the WeD-1 Pro (Fig. 1), an integrated multi-terminal platform with an AI-powered assistant for molecular POCT testing. Weighing only 290 g, the system features a newly engineered focal filter

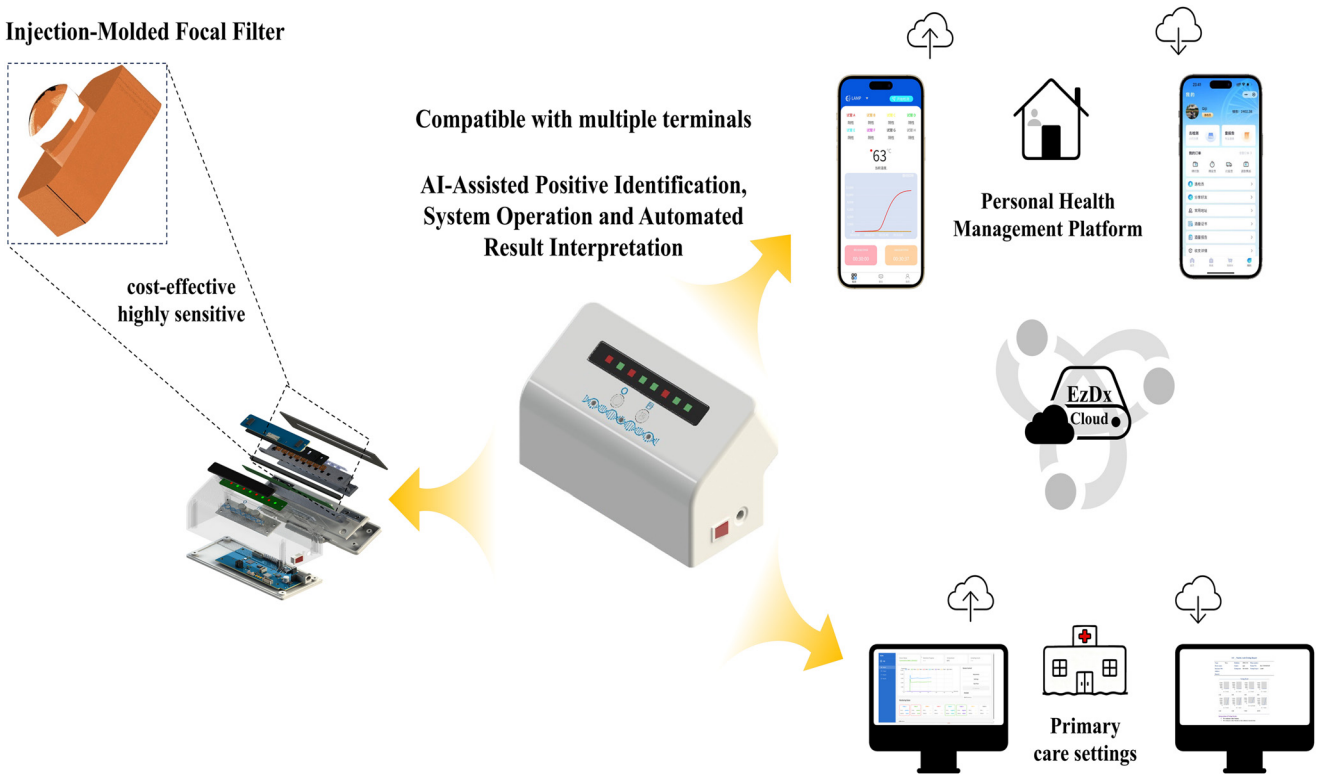

Fig. 1 Overview of the WeD-1 Pro system, injection-molded focal filter, and AI-powered workflow. The WeD-1 Pro is an integrated, multi-terminal platform designed for molecular point-of-care testing (POCT), featuring an injection-molded focal filter to enhance fluorescence detection. The system leverages an AI-powered workflow for seamless data capture, result interpretation, and automated reporting, offering a streamlined solution for both healthcare professionals and individual users. In this study, "multi-terminals" refer to smartphones, tablets, laptops, and desktop computers.

fabricated *via* injection molding, using a high-transmittance polycarbonate (PC) matrix blended with a custom high-temperature-resistant organic optical filter medium. This design enables low-cost, highly sensitive molecular fluorescence analysis. The platform supports seamless multi-terminal operation—including smartphones, tablets, laptops, and desktop computers—and is fully compatible with iOS, Android, macOS, and Windows systems. To facilitate reliable use by non-professional users, the WeD-1 Pro integrates an AI assistant that provides intelligent positive identification, step-by-step operational guidance, and automated result interpretation. Enhanced backend connectivity enables automated reporting and eliminates manual result analysis, with all reports stored in a relational MySQL database. These data can be further leveraged for statistical analysis of epidemic pathogens and machine learning-enabled pathogen alerts.

For individual users, beyond diagnostics, the WeD-1 Pro seamlessly integrates with personal health management platforms, establishing secure, bidirectional connections with healthcare services. It synchronizes health data to personalized dashboards and allows users to share results with medical professionals for remote consultations. For primary care settings, we developed a web-based application that allows the WeD-1 Pro platform to capture patient information *via* barcode scanning—using either a handheld scanner or a desktop/laptop camera. The system also supports the automatic generation of PDF reports, enabling physicians to save, print, and sign reports seamlessly. This streamlined workflow enhances clinical efficiency and ensures standardized documentation for medical records. Taken together, the WeD-1 Pro molecular POCT platform represents a transformative step toward precision diagnostics, with the potential to revolutionize both at-home testing and primary care applications.

2. Materials and methods

Injection-molded focal filter

The focal filter was designed with a radius of curvature of 2 mm and a center thickness of 3.18 mm (Fig. S1a). It consists of a mounting section and a focusing section. The mounting section is used to connect the filter to external components and also serves to protect the focusing section.

The focal filter was fabricated by injection molding using high-transmittance polycarbonate (PC; melt temperature: 270–310 °C; refractive index: 1.584–1.586) or polymethyl methacrylate (PMMA; melt temperature: 200–250 °C; refractive index: 1.490–1.492), blended with high-temperature-resistant pigments, including tailored phthalocyanine blue, quinophthalone, and benzimidazolone. These pigments selectively block 480 nm excitation light while allowing fluorescence transmission in the 510–650 nm range. Pigment masterbatches—comprising transparent color-filter agents, carrier resins, dispersants, and stabilizing additives—were sourced from Ampacet Corporation.

The injection mold was designed using Creo (Pro/E) and fabricated from NAK80, a pre-hardened, age-hardening, mirror-grade mold steel produced by Daido Steel, Japan. Injection molding was performed using an Engel E-motion 80 T machine. For formulation screening, pigment loadings ranging from 1 to 6 wt% were systematically assessed; respective barrel processing temperatures were set to approximately 240 °C for PMMA and 290 °C for PC.

Hardware platform: WeD-1 Pro instrument

Construction design. The internal components of the device include an aluminum alloy heating block, a custom PCB insulation cover, an optical filter mounting plate, a magnetic attraction assembly, and a series of electronic elements, such as an STM32 microcontroller (MCU), a high-brightness excitation light source, an ambient light sensor for fluorescence detection, and a Bluetooth module. In the prototyping phase, rapid prototyping was achieved using the Flashforge Guider II 3D printer in conjunction with nylon material, followed by precision machining of the components *via* computer numerical control (CNC) to ensure tight and seamless assembly of all parts. The aluminum alloy heating block, designed in SolidWorks, was fabricated using CNC processes, whereas the high-pass optical filter was formed *via* injection molding, with dimensions of 3.18 mm thickness × 7 mm length × 6 mm width. Details of the WeD-1 Pro construction design are illustrated in Fig. 2.

Thermal module design. The core heating assembly incorporates a custom PTC heater with a resistance of 7.5 Ω (sourced from Ming Sheng Hua Company), positioned between heating blocks A and B. The thermistor employs a Murata NTC thermistor with a negative temperature coefficient (*B*-value) of 3380 K. Heating regulation and switching management are achieved through an N-channel MOSFET (model AOD4184A, supplier: Alpha & Omega Semiconductor) using pulse-width modulation (PWM) waveforms. Concurrently, a 10 kΩ high-precision resistor (model RT0603BRD071KL, supplier: Yageo Corporation) works in tandem with the thermistor, enabling real-time temperature feedback *via* an analog-to-digital converter (ADC) to ensure precise temperature control. The printed circuit board was designed using the LCEDA online platform (Shenzhen, China) and manufactured by JLCPCB (Shenzhen, China).

Power module design. The power module primarily consists of a primary buck DC–DC voltage conversion circuit, utilizing a high-efficiency synchronous buck DC–DC converter chip SCT1450STER (from Qinheng Microelectronics, Nanjing, China) that supports a 5 A current output. The secondary buck stage comprises a low-dropout (LDO) linear regulator circuit, featuring an RT9193-33GB LDO chip (from Richtek Technology, Taiwan, China) that provides a stable 3.3 V output, paired with a REF3030AIDBZR chip (from Texas Instruments, Texas, USA) to supply an independent and stable 3.3 V voltage reference for the ADC

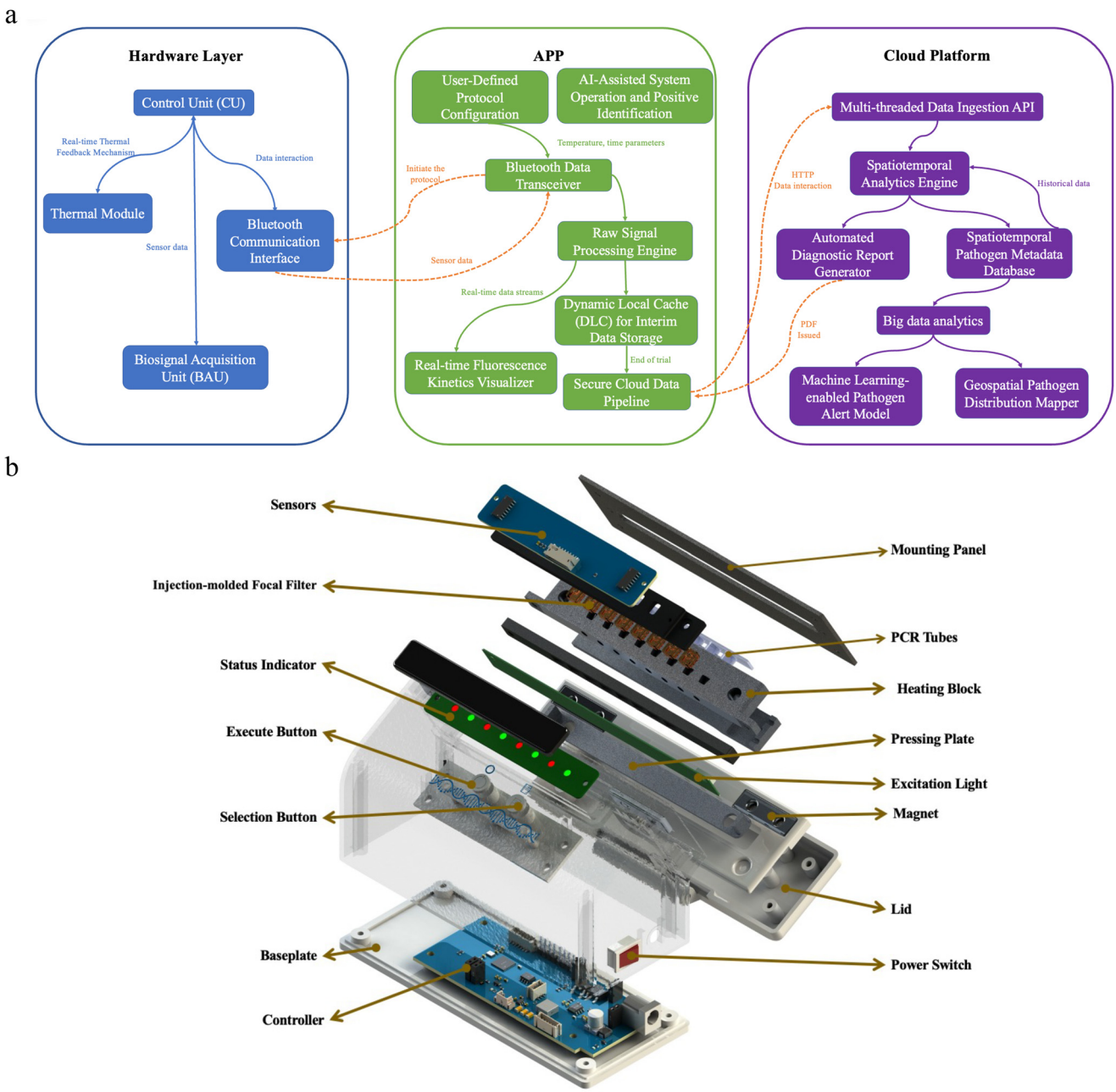

Fig. 2 Overview of the WeD-1 Pro system design and hardware components. (a) System architecture illustrating the integration of the hardware layer, which includes the real-time control unit with thermal feedback; the app interface, featuring Bluetooth data transceivers, fluorescence kinetics visualizer, and AI assistant; and the cloud platform, which integrates the data ingestion API, diagnostic report generator, and spatiotemporal analytics engine. (b) 3D exploded view of the device, showcasing five functional modules: optical unit, thermal module, power management unit, connectivity module, and standalone operation module, all centrally managed by the main control PCB for compact architecture, stable performance, and efficient system operation.

interface. This configuration facilitates more accurate thermistor sampling, forming the foundation for high-precision temperature control.

Optical module design. In the optical module, high-brightness blue LEDs (model SMD2835, 0.5 W) from Hongxinyuan Electronics (Shenzhen, China) were used as excitation sources. The system incorporates eight LEDs ($\lambda \approx$ 480 nm), each controlled independently through dedicated GPIO (general-purpose input/output) ports. To provide thermal insulation and prevent light leakage, an additional PCB with eight cutouts serves as a barrier layer.

Fluorescence signals are detected by eight ambient light sensors (ROHM, Japan) that were adaptively modified for this application. To minimize interference from excitation light, the LEDs and sensors were arranged perpendicularly (Fig. 2). Furthermore, eight high-pass injection-molded focal filters (500–670 nm) were installed in front of the sensors, effectively blocking the 480 nm excitation

wavelength while transmitting and focusing the emission signals.

Connectivity module design. The Bluetooth low energy (BLE) module was supplied by Qinheng Microelectronics (Nanjing, China). The module, measuring 10.6 mm × 10.2 mm, supports Bluetooth version 4.2, features ultra-low sleep power consumption of just 1 μA, and offers a maximum transmission range of 100 m. Data transmission is configured through this BLE module, with a set of data structures serving as the interface for communication between the device and a mobile phone.

Multi-terminal software architecture

To enable cross-platform use, the system was built with the Uni-app framework (based on Vue.js) and integrates the Web Bluetooth API for device connectivity. It supports both iOS and Android mobile apps for immediate on-site testing and data entry, as well as a browser-based interface for PCs and hospital information systems to facilitate streamlined workflow management.

Automatic PDF report generation

Data reception and validation module. Real-time detection data from WeD-1Pro devices are transmitted *via* Bluetooth to mobile devices or PCs. The data, structured in JSON format, includes metadata such as assay type, reaction temperature, reaction duration, geographical coordinates (latitude/longitude), and assay results. These data packets are received by the backend through Spring Boot-based RESTful APIs and are deserialized using the Jackson library. Upon receipt, each dataset undergoes a comprehensive validation process to ensure data integrity and compliance with the prescribed formats. Only validated data are processed in the subsequent stages.

Data processing and report generation module. Upon data reception, the system implements a multi-stage validation protocol to ensure data integrity and compliance with predefined formats. Subsequently, analytical pipelines apply domain-specific business rules to classify each assay result as positive or negative, leveraging clinically validated thresholds (*e.g.*, cutoff values derived from statistical distributions of negative/positive controls). Following data analysis, the system initiates an automated report generation pipeline *via* the Apache POI library. Reports adhere to standardized templates, incorporating critical fields such as: testing items, threshold cycle values (Ct), reference ranges, and diagnostic interpretations (positive/negative). The finalized reports are exported in PDF format, with unique access links dynamically returned to the frontend application. This enables end-users to seamlessly retrieve or download diagnostic reports through secure channels.

Data storage and management module. All acquired assay data are persisted in a MySQL database structured with a normalized relational schema. Database tables incorporate key fields including device identifiers, detection timestamps, geospatial coordinates, assay identifiers, and assay results. To optimize query efficiency, indexing strategies are implemented on frequently queried fields such as device identifiers and assay types. Data persistence operations utilize Spring Data JPA, ensuring efficient data access and management under high-concurrency conditions.

Geospatial visualization module. The system integrates the Amap API to enable real-time visualization of detection device locations. Geospatial coordinates from each device are transmitted to the EzDx Cloud frontend,[5] triggering dynamic updates to the map, including device positions and regional assay results. This module also supports the development of machine learning-enabled pathogen alert models.

AI-assisted positive identification

The proposed model leverages a bidirectional long short-term memory (BiLSTM) network integrated with an Attention mechanism for the automatic classification of nucleic acid amplification curves. It was trained on a dataset of 1000 RPA and 1000 LAMP results, selected by an experienced researcher from the backend database of the EzDx Cloud platform. The classification of RPA and LAMP data is based on reaction temperature. The overall architecture is detailed below:

(1) Feature enhancement. Each time step is transformed into a 4-dimensional feature vector:

$$\mathbf{x}_t^{\text{enh}} = \begin{bmatrix} x_t \\ \Delta x_t \\ \Delta^2 x_t \\ \text{rolling\_mean}_t \end{bmatrix} \in \mathbb{R}^4,\ t = 1,\ 2,\ \ldots,\ T$$

where:

- $\Delta x_t = x_t - x_{t-1}$ (first-order difference)
- $\Delta^2 x_t = x_t - x_{t-1}$ (second-order difference)
- rolling_mean_t smooth local noise.

(2) BiLSTM layer. The BiLSTM generates forward and backward hidden states:

$$\overrightarrow{h_t} = \text{LSTM}_{\text{forward}}\left(x_t, \overrightarrow{h_{t-1}}\right),\ \overleftarrow{h_t} = \text{LSTM}_{\text{backward}}\left(x_t, \overleftarrow{h_{t+1}}\right)$$

The final hidden representation:

$$h_t = \left[\overrightarrow{h_t}; \overleftarrow{h_t}\right] \in \mathbb{R}^{2\text{H}}$$

(3) Attention mechanism. Attention weights are computed as:

$$e_t = \mathbf{w}^{\text{T}} h_t,\ \alpha_t = \frac{\exp(e_t)}{\sum_{k=1}^{T} \exp(e_k)}$$

The context vector aggregates weighted hidden states:

$$c = \sum_{t=1}^{T} \alpha_t h_t$$

Intuitively, a_t highlights the contribution of each time step to the final classification.

(4) Classifier. The context vector c is passed through a multi-layer perceptron (MLP):

$$y_{\text{hat}} = \text{Softmax}(W_2\text{ReLU}(W_1 c))$$

The output $y_{\text{hat}} \in \mathbb{R}^3$ represents the probabilities for negative, weak positive, and strong positive classes.

AI assistant

The agent, developed using the LangChain and LangGraph frameworks, features a Manager Node that centrally routes user queries to specialized nodes through large language model (LLM)-driven analysis and structured prompting (Fig. S2). These specialized nodes include:

- a **RAG_Expert node**, which performs knowledge base question & answering using BGE-small-zh-v1.5 embeddings and bge-reranker-base for query rewriting, vector database retrieval, re-ranking, and answer synthesis;
- a **DB_Expert node**, which executes a ReAct-based iterative process (Plan–Act–Observe cycles) for SQL query generation and test data retrieval, followed by structured tabular result presentation; and
- a **Chat_Expert node**, which provides direct conversational responses through an LLM interface.

Processed outputs are ultimately delivered to users through the system's application interface for presentation and interaction.

Development of a nine-pathogen detection panel for common respiratory infections based on one-tube/one-step LAMP-CRISPR assay

Previously, we developed a pioneering one-tube/one-step LAMP-CRISPR assay, leveraging the newly engineered thermostable AapCRISPR-Cas12b variant, ScCas12b.[2] In this study, we expanded our approach to comprehensively detect prevalent respiratory pathogens by developing a nine-pathogen detection panel based on the one-tube/one-step LAMP-CRISPR assay. The primer set for HRV was designed in-house, while primer sets for other pathogens were sourced from published literature (Table S1). Additionally, novel sgRNAs were designed for each of the nine pathogens (Table S2). The LAMP-CRISPR assay utilizes a total reaction volume of 25 μL, containing the following components: 1X LAMP isothermal buffer (New England Biolabs, US), 1X primer mix, 8 U BST 2.0 (SignalChem Biotech Inc., Suzhou), 24 nM Cas12b, 25 nM sgRNA, 500 nM ssDNA reporter, 6 mM $MgSO_4$, and 1 U AMV (Promega, US). All reagents were lyophilized, and the performance of the lyophilized formulations was further evaluated (see SI for detailed results). For rapid pathogen detection, nasal swabs were collected into LAMP-compatible rapid lysis buffer (provided by Hangzhou EzDx Technology Co., Ltd). A 25 μL aliquot of the lysed sample was added to the lyophilized reagents, and the reaction mixture was incubated in the WeD-1 Pro system at 65 °C for 30 minutes.

3. Results

3.1. Overall design of the WeD-1 pro IoT detection system

The WeD-1 Pro detection system is an advanced Internet of Things (IoT) solution, consisting of three key layers as shown in Fig. 2a: the hardware layer, which includes a real-time control unit with thermal feedback; the app interface, which features Bluetooth data transceivers, a fluorescence kinetics visualizer, and an AI assistant; and the cloud platform, which integrates a data ingestion API, diagnostic report generator, and spatiotemporal analytics engine.

3.2. Overall design and module validation of the WeD-1 Pro hardware

Overall design. The WeD-1 Pro integrates five functional modules, all centrally managed by a main control PCB. These include an optical unit for excitation and fluorescence detection, a thermal module for precise temperature regulation, a power management unit, a connectivity module, and a standalone operation module. Each module is seamlessly embedded into the base of the main control PCB, ensuring compact architecture, stable performance, and efficient system operation (Fig. 2b).

Thermal module. The device is equipped with a thermal control system capable of heating within a range of 35 °C to 100 °C, with a precision of ±0.3 °C (Fig. S3). This broad and accurate temperature range supports a variety of isothermal amplification assays, including high-temperature LAMP-PfAgo reactions. The module achieves rapid thermal response, reaching 65 °C from room temperature in approximately 56 seconds (Video S1), which corresponds to the optimal reaction temperature for LAMP and LAMP-CRISPR assays.

Standalone operation module. The WeD-1 Pro incorporates an independent result indication module with LED indicators, along with a selection button and execution button for standalone operation (Video S2). The test results are displayed through the LED indicators. The "selection button" allows users to switch among built-in reaction programs, which are typically preset with common reaction temperatures and durations. These include isothermal amplification methods such as Recombinase Polymerase Amplification (RPA) and Loop-Mediated Isothermal Amplification (LAMP), with flexibility for user-defined customization. Upon completion, the system automatically interprets fluorescence data and provides semi-quantitative analysis: red illumination indicates a positive result, with the intensity of the redness correlating to higher target concentrations, while green indicates a negative result (Video S2). In addition to reporting outcomes, the LEDs offer real-time feedback on both temperature and reaction progress. Color changes correspond to heating thresholds, and sequential illumination signals the passage of time.

Injection-molded focal filter. Current molecular POCT devices typically rely on two glass components—optical filters and convex lenses. Although these glass-based filters use

specialized coatings for fluorescence filtering, the coatings are prone to scratching and gradual deterioration, which increases maintenance demands and costs. Moreover, these two glass components are expensive, difficult to manufacture, and increase the overall device volume—factors that add complexity and limit their suitability for cost-sensitive applications.

To overcome these challenges, we developed and integrated a custom focal filter (Fig. 3a, left and b) into the optical detection module. To optimize the filtering performance, we systematically screened (n = 3) various polymer substrates and organic optical filter media (pigment). As shown in Fig. 3c, compared to quinophthalone (QP) and benzimidazolone (BIG) pigments, the tailored phthalocyanine blue (Pc blue) pigment exhibited the best ability to block 480 nm excitation light and provided optimal transmission of 525 nm light when mixed with polycarbonate (PC). In contrast, when mixed with polymethyl methacrylate (PMMA), the same pigments showed significantly lower 480 nm excitation light blocking efficiency. We hypothesize that

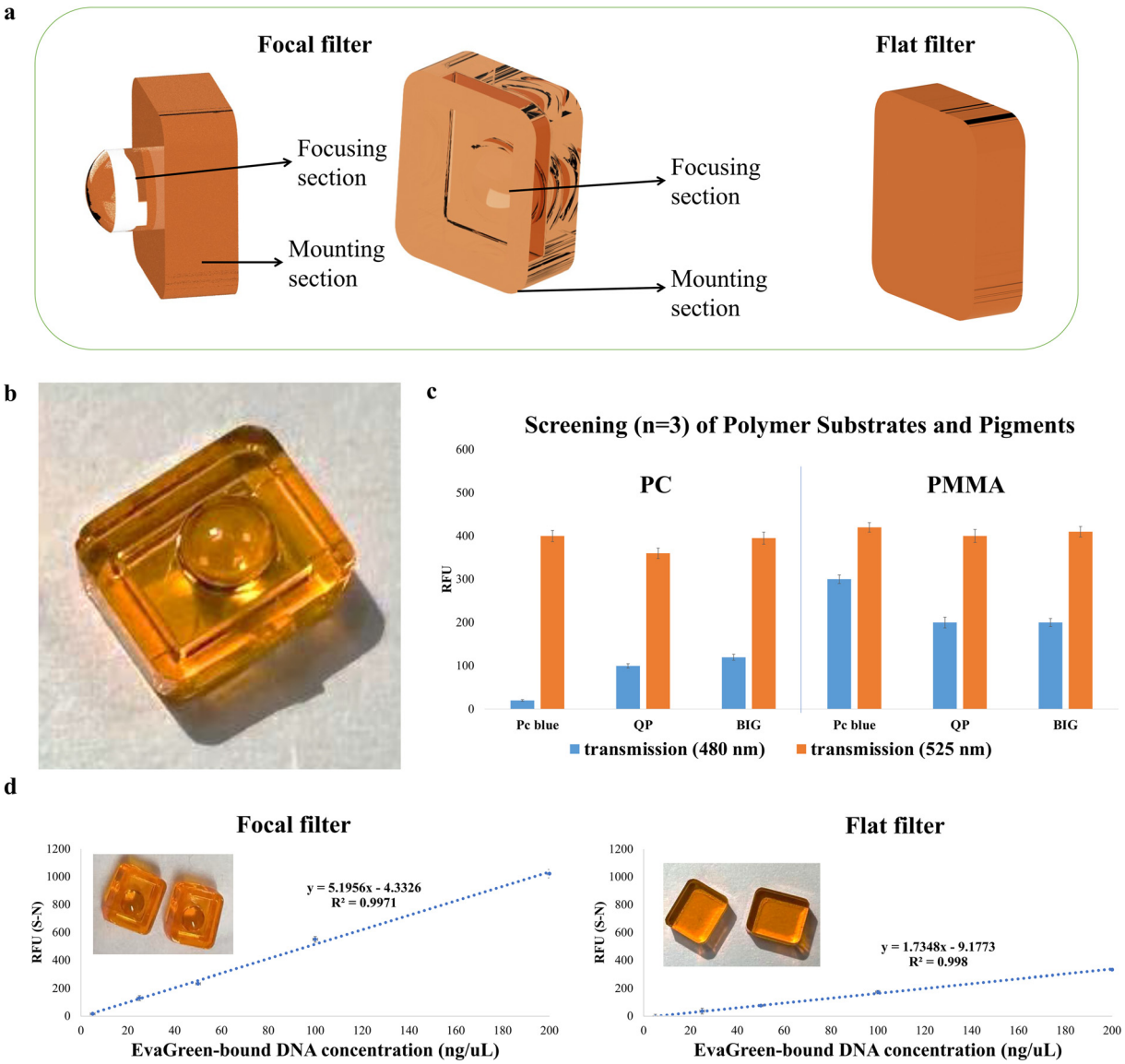

Fig. 3 Comparison of focal and conventional flat filters in molecular POCT devices. (a) Schematic representation of the focal filter, an integrally molded polycarbonate component with a focusing section (incorporating a built-in convex lens) and a mounting section, contrasted with the conventional flat filter. (b) Images of the fabricated focal and flat filters. (c) Screening of polymer substrates and pigments. The WeD-1 Pro device was used to evaluate the optical performance of different polymer–pigment formulations. LEDs with peak wavelengths of approximately 480 nm and 525 nm were employed to simulate excitation and emission light, respectively. A pigment concentration of 4 wt% Pc blue was used. Each measurement was performed in three independent replicates to ensure statistical robustness. (d) Linear regression analysis of relative fluorescence units (RFU, S–N), where S represents the fluorescence intensity from the target substance and N denotes background noise from blank samples (baseline fluctuation), *versus* EvaGreen-bound DNA concentration. The focal filter exhibits a steeper slope (y = 5.1956x − 4.3326, R^2 = 0.9971) compared to the flat filter (y = 1.7348x − 9.1773, R^2 = 0.998), indicating enhanced sensitivity. The graphs depict the RFU (S–N) values from three independent experiments, highlighting the focal filter's consistent superior performance across varying EvaGreen-bound DNA concentrations.

this discrepancy is due to differences in how the polymer structure affects the conjugated structure of the pigments. Statistical significance was confirmed by one-way ANOVA (Fig. S1b). Based on the results, a high-transmittance, high-temperature-resistant PC polymer combined with Pc blue was selected as the optimal formulation. We further evaluated pigment concentration during optimization, as shown in Fig. S1c, testing 1, 2, 4, and 6 wt% Pc blue. Increasing pigment concentration enhanced 480 nm excitation blocking, but excessive loading reduced 525 nm emission transmission and negatively affected optical clarity and processability. Considering the balance between excitation blocking and emission transmission, 4 wt% Pc blue was selected as the optimal formulation.

The resulting focal filter is produced *via* a single-step injection molding process and fabricated as a monolithic component that incorporates both the focusing element and the mounting structure (Fig. 3a, left and b). The focusing section incorporates a built-in convex lens that collects and converges the emitted fluorescence signals onto the sensor's photosensitive area, while the high-temperature organic color-filter agents in the medium effectively absorb incident excitation light.

To clarify the contribution of the focusing structure, a flat filter composed of the same material was fabricated as a control (Fig. 3a, right; Video S3). Filters were installed in front of the sensors of the WeD-1 Pro device to evaluate optical performance. Compared with the conventional flat filter, the focal filter substantially enhanced signal acquisition efficiency, yielding higher RFU values and a markedly steeper concentration–response slope ($y = 5.1956x - 4.3326$ *vs.* $y = 1.73348x - 9.1773$) (Fig. 3d). Moreover, the focal filter achieved a limit of detection (LOD) of 5 ng μL^{-1} for EvaGreen-bound DNA, representing an approximately threefold improvement over the 15 ng μL^{-1} LOD of the flat filter. Notably, this enhancement was achieved while maintaining relatively stable background noise (Fig. S1d), thereby significantly improving the signal-to-noise ratio (SNR).

To further substantiate the optical performance of the injection-molded focal filter, we performed a matched comparison using a commercially available glass optical filter under identical detection conditions, including the same excitation source, fluorescent sample, detector, optical path, and acquisition settings. The commercially available glass optical filter demonstrated optical performance comparable to that of the injection-molded flat filter, with a limit of detection (LOD) of 15 ng μL^{-1} for EvaGreen-bound DNA. Despite this comparable analytical performance, its estimated component cost (approximately US$3.50 per unit) was approximately seven-fold higher than that of the injection-molded filter (Table S3). Compared with conventional fluorescence optical configurations that require separate coated-glass filters and lenses,[8,9] the injection-molded focal filter integrates optical filtering and focusing into a single PC-based component. This design reduces cost, simplifies alignment, improves miniaturization, and enhances handling robustness. As shown in Table 1, the focal filter effectively blocked 480 nm excitation light, with an OD of 3.2 ($T = 0.063\%$), while maintaining 90% transmittance at 525 nm and reducing the estimated component cost to less than US$0.50. These results support its use as a compact and low-cost alternative to conventional glass-filter-based optical configurations in fluorescence POCT systems.

3.3. Multi-terminal software architecture and operation procedure

To enable multi-platform compatibility across iOS, Android, laptops, and PCs, we developed a cross-platform application using Uni-app.

Mobile device application. The main interface for individual users features a single Home Page with seven key icons: "Connect WeD-1 Pro", "Start Run", "Generate Report", "Add New Project", "Traceback Data", "AI Assistant", and a "Scanning" icon (Fig. 4a-i). Among these, two icons trigger pop-up windows: "Add New Project" for project management (Fig. 4a-ii) and "Start Run" for entering tester/testee and sample information, as well as selecting the testing program (Fig. 4a-iv). Through the "Add Item" option, users can customize project settings such as project name, reaction temperature, reaction duration, and target identifier (Fig. 4a-iii).

Web application. For PC and laptop use, a browser-based interface was developed by integrating the Web Bluetooth API to enable seamless device connectivity (Fig. 4b). This is particularly well-suited for primary care environments, as it

Table 1 Comparison of the injection-molded focal filter and conventional optical configuration

Parameter	Injection-molded focal filter	Conventional optical configuration[8, 9]
Optical structure	Integrated filter and focusing section	Separate flat filter and convex lens
Main material	PC with optical pigment	Coated glass filter + lens
Fabrication	Single-step injection molding	Separate filter/lens manufacturing and assembly
Estimated component cost	Lower/<$0.5 per unit	Higher/$5–150 per unit
Component number	One integrated component	Two or more components
Miniaturization	Higher, compact integrated design	Limited by alignment and assembly
Alignment requirement	Reduced	Requires filter-lens alignment
Mechanical robustness	Better handling resistance/less fragile	Glass component is fragile
Batch reproducibility	High	Manufacturer-specified spectral tolerance
Excitation blocking	480 nm blocked, OD = 3.2, $T = 0.063\%$	480 nm blocked, OD > 3.0, $T < 0.100\%$
Emission transmission	510–650 nm transmission, 525 nm: $T = 90\%$	525 nm: >84%

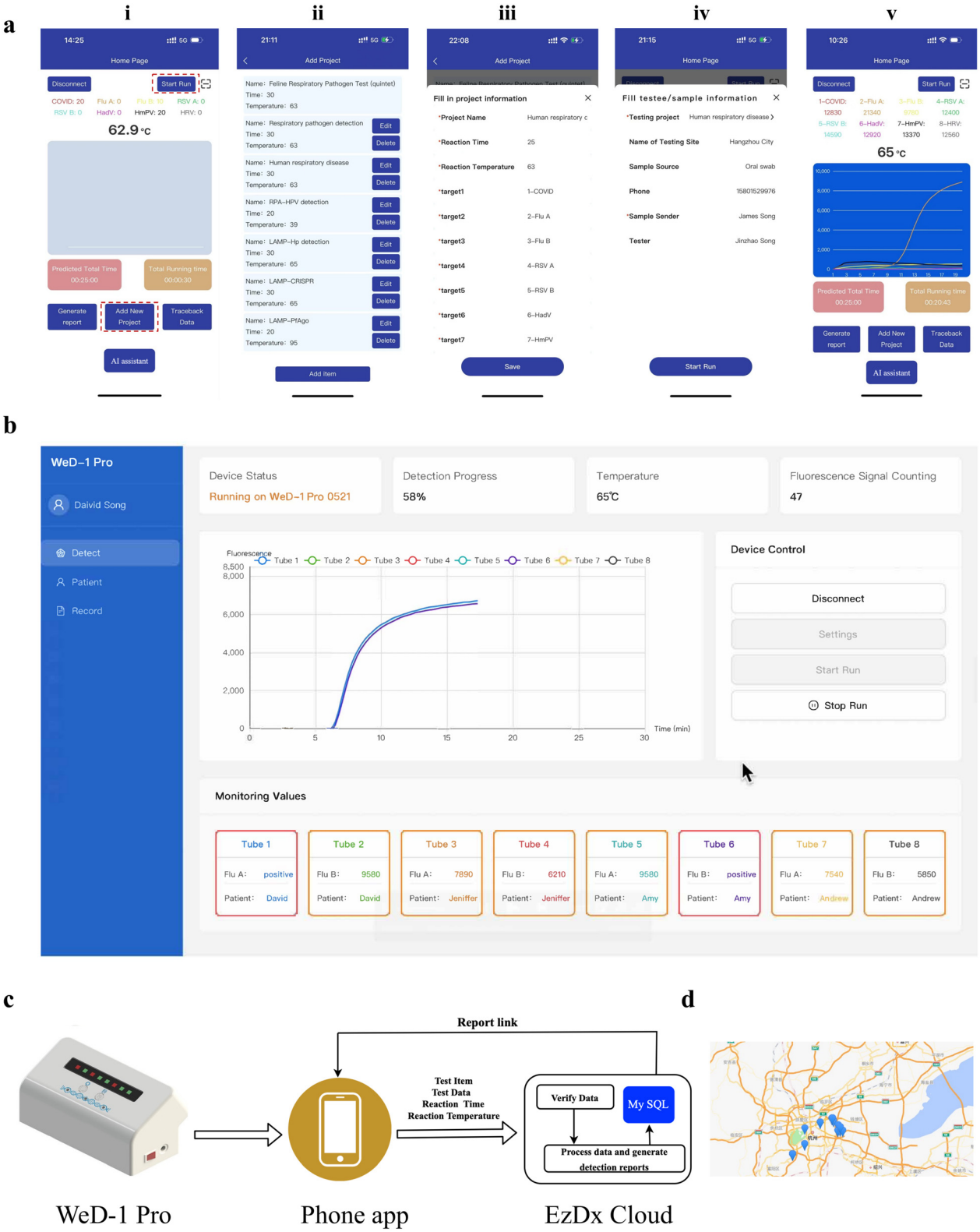

Fig. 4 Multi-terminal software architecture and operation procedure of the WeD-1 Pro system. (a) Mobile app interface showing key icons for system operation: "Connect WeD-1 Pro", "Start Run", "Generate Report", "Add New Project", "Traceback Data", "AI Assistant", and "Scanning". Pop-up windows are triggered for project management and entering tester/sample information. (b) Browser-based web interface for PC/laptop use, integrating the Web Bluetooth API for device connectivity, suitable for primary care environments. Features include barcode scanning for rapid patient and sample information retrieval, and automatic PDF report generation. (c) Overview of the system's processing flow, including backend architecture with a MySQL database, data acquisition, storage, analysis, and reporting modules, and integration with the Amap API for real-time geospatial visualization. (d) Geospatial visualization of detection activities, showing real-time updates of device locations and assay results.

eliminates disruptions from calls or notifications. It also allows primary care staff to perform concurrent tasks and immediately update electronic medical records (EMR) with a dedicated barcode scanning function. This feature facilitates the rapid retrieval of patient and sample information using either a handheld scanner or a phone/desktop/laptop camera (Video S4). The PC interface allows patient registration, assigns different testing items and patient names to each reaction well, and generates personalized reports for multiple patients in a single run (Fig. S4 and Video S5).

Automatic PDF report generation. The system's processing flow is depicted in Fig. 4c. The backend architecture of EzDx Cloud is built using the Spring Boot framework, with data storage managed through a MySQL database. Integration with the Amap API enables real-time visualization of geospatial data, facilitating spatiotemporal monitoring of detection activities (Fig. 4d). The backend consists of four main modules: data acquisition, data storage, analysis & reporting, and geospatial visualization. Communication between these modules occurs *via* standardized RESTful interfaces, ensuring scalability, robustness, and high efficiency. The automatic generation of PDF reports is demonstrated in Videos S5 and S6.

App operation procedure. To run an assay, open the app, where the Bluetooth ID will be automatically detected. Then, click "Start Run", select a testing project, input the necessary information, and press the internal "Start Run" button to begin the process. Positive and negative results are determined based on either the preset threshold or our trained AI algorithm. Notably, our algorithm provides immediate indication of positive results during the reaction (Video S5). Once the experiment is complete, the app automatically generates a PDF report (Videos S5 and S6). The fluorescence data and corresponding time points are temporarily stored on the device and synchronized with the smartphone upon reconnection, allowing amplification curves to be redisplayed for further analysis (Videos S5 and S6).

3.4. AI-assisted positive identification and system operation

AI-assisted positive identification. Conventional threshold-based methods for determining positive results have several limitations. Amplification curve patterns differ substantially between RPA and LAMP. LAMP-positive results typically display a characteristic sigmoidal curve, whereas negatives may show a slow, gradual rise. In contrast, RPA curves—particularly for low-concentration samples—often exhibit a gradual slope similar to LAMP-negative reactions, complicating the establishment of universal thresholds. Even linear regression and second-derivative analyses cannot reliably account for variations in curve morphology across amplification methods. Additionally, fluorescence intensity within a single method can vary depending on dye type and concentration, making accurate interpretation challenging for first-time users and even some experienced researchers.

To address this issue, we developed an AI-based model utilizing a bidirectional long short-term memory (BiLSTM) network integrated with an Attention mechanism for the automatic classification of nucleic acid amplification curves. The model begins by classifying amplification techniques based on the reaction temperature field in the data: samples with reaction temperatures between 37 and 42 °C are categorized as RPA data, while those in the 60–65 °C range are classified as LAMP data. The model was trained on a dataset of 1000 RPA and 1000 LAMP results. For ground-truth labeling, conventional PCR was employed to determine the positive and negative status of each sample. The corresponding amplification curve patterns were then mapped one-to-one to their validated "Positive" and "Negative" labels, enabling supervised training of the model. This process generated clearly annotated subsets of positive and negative samples for both RPA and LAMP reactions. The overall architecture of the model is illustrated in Fig. 5a and comprises bidirectional temporal feature extraction, attention-based weighting for key feature emphasis, and fully connected classification layers. During operation, the model automatically identifies the amplification method (RPA or LAMP) based on reaction temperature and subsequently determines the test outcome (positive or negative) according to characteristic amplification curve patterns.

To rigorously evaluate the model's performance, in addition to the 2000 training samples, an independent validation dataset comprising 600 amplification curves with corresponding PCR results was used, including 300 RPA and 300 LAMP reactions with an equal distribution of positive and negative cases. These data were not used for model training, hyperparameter tuning, or model selection. To reflect the statistical distribution of the dataset, the confusion matrix for the test set is provided in Table S4. In addition, weak-positive, late-amplification, and morphologically ambiguous curves were analyzed as challenging subgroups to assess model robustness (Table S5). Using the same validation dataset, we compared the BiLSTM-Attention model with three conventional curve-classification methods: baseline-corrected threshold crossing, linear-regression-based slope analysis, and second-derivative analysis of amplification amplitude. Compared with conventional PCR results, the AI model-based method achieved an overall accuracy of 100% (95% CI: [98.2%, 100.0%]) without requiring manually defined thresholds. In contrast, without method-specific classification, the accuracies of baseline-corrected threshold crossing, linear-regression-based slope analysis, and second-derivative analysis were 92.0%, 95.0%, and 96%, respectively (Table S6). ROC curve analysis demonstrated that the model accurately differentiated positive and negative reactions, achieving an AUC of 1.00 (95% CI: [0.995, 1.000]), whereas the baseline-corrected threshold crossing, linear-regression-based slope analysis, and second-derivative analysis yielded AUCs of 0.962, 0.975, and 0.982, respectively (Fig. 5b). Notably, the model also maintained reliable classification performance for

a

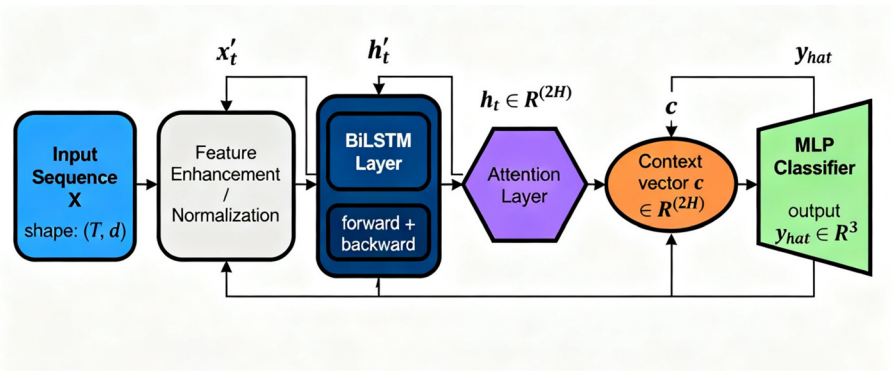

b

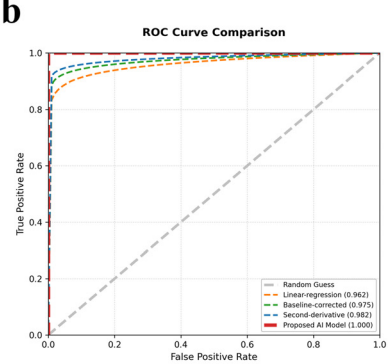

c

Knowledge Category	Average Score
Qwen-max	2.481
Knowledge Q&A Function (Qwen-max + original)	3.594
Knowledge Q&A Function (Qwen-max + fine-tuning)	3.769

d

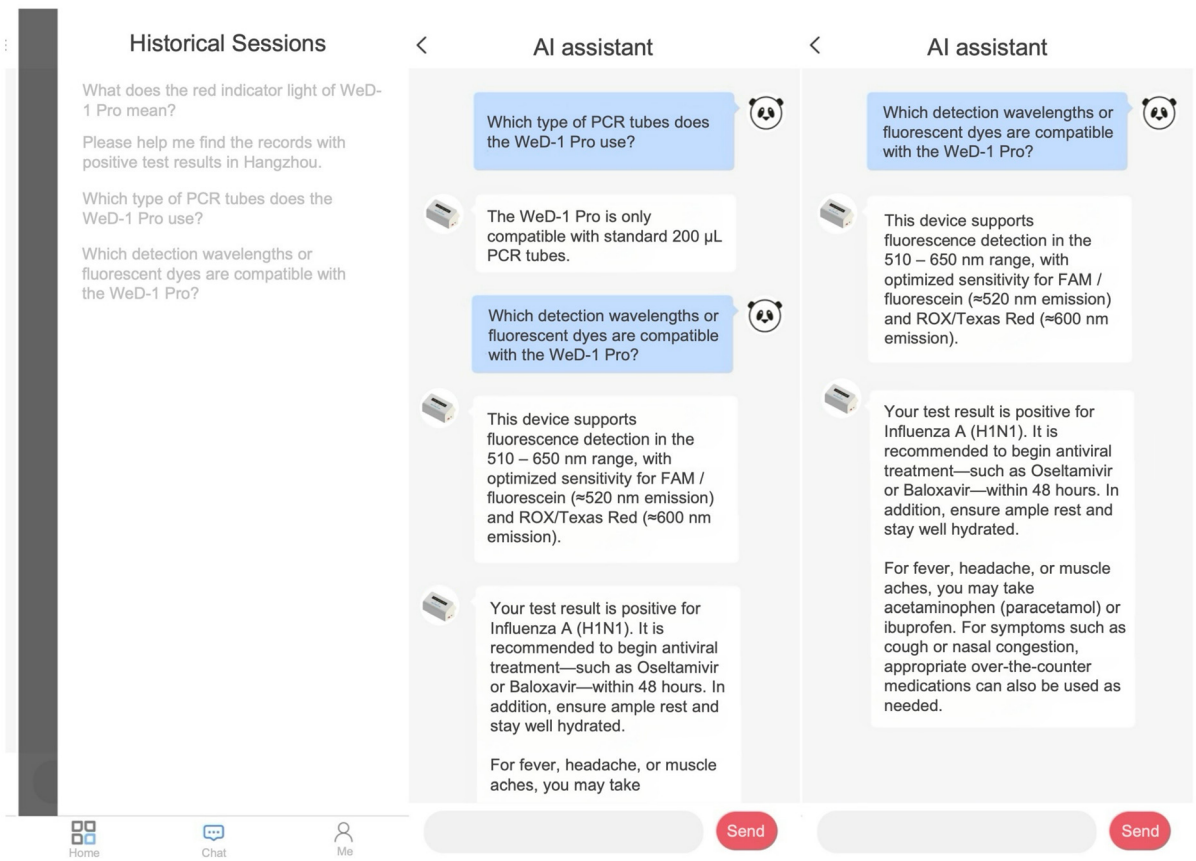

Fig. 5 AI-assisted positive identification and system operation. (a) The overall architecture of the AI-based model. (b) ROC curve comparison of the proposed BiLSTM-Attention AI model and three conventional curve-classification methods for differentiating positive and negative reactions. The proposed AI model achieved the highest discriminative performance with an AUC of 1.000. (c) Performance comparison between the original RAG system and standalone Qwen-max LLM on 160 molecular diagnostic questions, with the RAG system achieving a 45% improvement in answer relevance. (d) Example of a user interaction with the AI assistant, showing the knowledge base Q&A function and real-time assistance during diagnostic tests.

weak-positive, late-amplification, and ambiguous amplification curves, supporting its robustness across different curve morphologies. Overall, these results suggest that a learning-based model is necessary to capture

method-specific curve morphologies and improve the robustness of result classification, particularly for weak-positive or atypical amplification curves.

AI-assisted system operation and automated result interpretation. The agent was developed using the LangChain and LangGraph frameworks. By incorporating a high-performance embedding model to enhance the retrieval stage, the relevance of the generated answers was significantly improved—this is because more accurate semantic retrieval provides the large language model (LLM) with more relevant contextual information. In tests involving 160 molecular diagnostic questions, the full retrieval-augmented generation (RAG) system substantially outperformed the standalone Qwen-Max LLM, achieving an average relevance score of 3.594 on a five-point scale—representing a 45% improvement over the baseline score of 2.481 (Fig. 5c). Furthermore, a fine-tuned multistage optimization pipeline—comprising query rewriting, vector retrieval, and bge-reranker-base-based reranking—further enhanced performance, yielding an additional ~5% increase

a

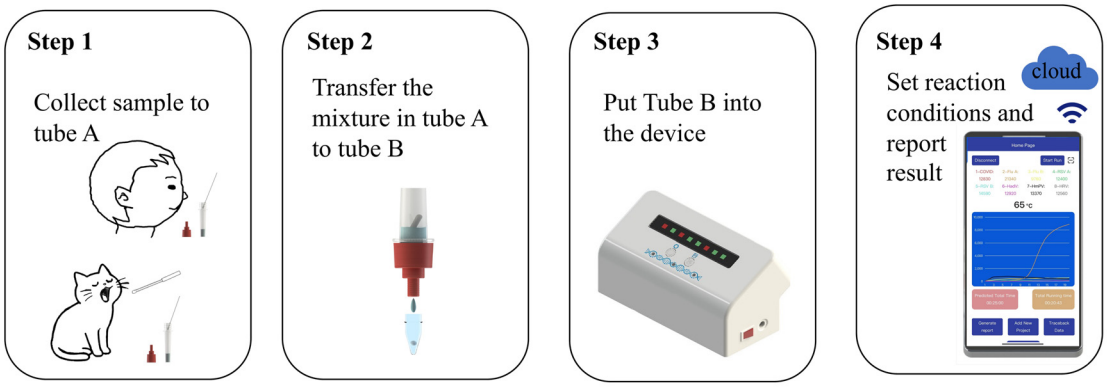

b

At-Home Detection of Common Respiratory Pathogens

	Patient NO.	Day 1	Day 2	Day 3	Day 4	Day 5
PCR Result and Ct Value	1	pos. 33	pos. 30	pos. 30	pos. 36	neg.
	2	pos. 32	NA	neg.	NA	NA
	3	pos. 34	NA	neg.	NA	NA
WeD-1 Pro Result and Tt Value	1	pos. 13	pos. 10	pos. 10	pos. 15	neg.
	2	pos. 11	NA	neg.	NA	NA
	3	pos. 13	NA	neg.	NA	NA

c

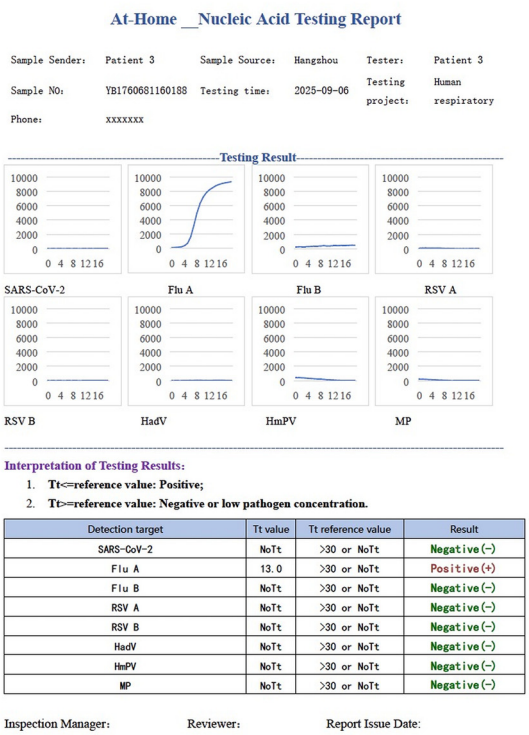

d

Identifying Feline Respiratory Pathogens in Small Veterinary Clinics

	C. psittaci	FCV	FIAV	MF	FHV	Bb	CF	Positive for at least one pathogen	Co-infections	Co-infections involving C. psittaci.	Total
Positive Rate	73%	38%	30%	22%	15%	9.8%	4.7%	87%	55%	45%	NA
Agreement with traditional PCR	100% (42/42)	96% (22/23)	100% (19/19)	100% (13/13)	100% (8/8)	100% (6/6)	100% (3/3)	NA	NA	NA	98% (59/60)

Fig. 6 At-home detection of human respiratory pathogens and on-site identification of feline respiratory pathogens using the AI-powered WeD-1 Pro system. (a) Workflow of the WeD-1 Pro system for the rapid detection of common respiratory pathogens using swabs and a proprietary rapid lysis buffer. (b) Comparison of results from the WeD-1 Pro device and a commercial qPCR kit for three individuals—one infected with SARS-CoV-2 and two with influenza A (flu A), showing 100% concordance. The SARS-CoV-2 infected individual exhibited dynamic viral titer changes over a four-day period without medication, while the flu A-infected individuals achieved viral clearance within 48 hours following oseltamivir treatment. (c) Automatically generated PDF testing reports sent to participants *via* the mobile app interface. (d) The EzDx 7-plex feline respiratory pathogen kit was used to identify FHV, FCV, *Bordetella bronchiseptica* (Bb), *Mycoplasma felis* (MF), *Chlamydia felis* (*CF*), feline influenza A virus (FIAV), and *Chlamydia psittaci* in 1000 tests conducted across 40 small veterinary clinics, with 87% of samples testing positive for at least one pathogen. Among the 1000 on-site veterinary tests, a subset of 60 samples was further compared with reference PCR, showing 98% concordance.

in answer relevance compared to the non-optimized RAG system (3.769 *vs.* 3.594). Fig. 5d illustrates a representative interaction scenario in which the system responds to a user's query *via* the knowledge base question–answering function during engagement with the AI assistant. User testing showed that 92% of novice individual users (n = 120) were able to complete diagnostic tests independently with the support of the AI assistant's task decomposition and real-time error intervention features; the remaining 8% successfully completed testing with video-call guidance.

3.5. At-home detection of common respiratory pathogens using the AI-powered WeD-1 Pro device

Distinguishing between respiratory pathogens in symptomatic individuals is of critical importance for guiding appropriate treatment. For example, oseltamivir has demonstrated strong efficacy in inhibiting the replication of both influenza A and B viruses. In contrast, *Mycoplasma pneumoniae* (MP) infections require specific antibiotic therapy, which is ineffective against viral pathogens such as influenza, RSV, or SARS-CoV-2. Previously, we established a one-tube/one-step LAMP-CRISPR assay for the detection of SARS-CoV-2 and H1N1. Building upon this foundation, we developed an expanded nine-respiratory pathogen detection panel capable of detecting the most common respiratory pathogens, including SARS-CoV-2 (severe acute respiratory syndrome coronavirus 2), flu A (influenza A virus), flu B (influenza B virus), RSV A (respiratory syncytial virus A), RSV B (respiratory syncytial virus B), HAdV (human adenovirus), HMPV (human metapneumovirus), HRV (human rhinovirus), and MP (*Mycoplasma pneumoniae*) (Fig. S5). The one-tube/one-step LAMP-CRISPR detection system achieved a limit of detection of 100 copies per reaction (Fig. S6), with 100% specificity confirmed by *in silico* analysis.

As illustrated in Fig. 6a, the workflow of the WeD-1 Pro/one-tube/one-step LAMP-CRISPR system enables convenient at-home identification of prevalent respiratory pathogens. Oral swab samples were collected from individuals presenting with respiratory symptoms and added to a proprietary rapid lysis buffer (from Hangzhou EzDx Technology Co., Ltd), which was verified to exert no inhibitory effect on the lyophilized LAMP and LAMP-CRISPR reagents. Subsequently, 25 μL of the resulting lysate was transferred into tubes preloaded with lyophilized reagents for immediate analysis. Monitoring three individuals (a 42-year-old adult, a 14-year-old girl, and a 9-year-old boy) using the AI-powered WeD-1 Pro device for detecting nasal swab samples revealed one case of SARS-CoV-2 infection and two cases of influenza A (flu A), demonstrating 100% concordance with results obtained from a commercial qPCR kit (Fig. 6b). The individual infected with SARS-CoV-2 exhibited dynamic changes in viral titer from symptom onset to recovery over a four-day period without medication, whereas both flu A-infected individuals achieved complete viral clearance within 48 hours following oseltamivir treatment (Fig. 6b and S7). All test results were automatically uploaded to the EzDx Cloud platform, enabling integrated health management, treatment guidance, and epidemiological disease mapping. Simultaneously, participants received automatically generated PDF testing reports through the mobile app interface (Fig. 6c).

3.6. Identifying pet pathogens in small veterinary clinics using the AI-powered WeD-1 Pro system

Clinical on-site detection of pet pathogens. With growing public awareness of pet health, molecular diagnostic technologies for at-home and on-site testing have become increasingly important. At-home testing allows pet owners to conveniently and promptly monitor their pets' health, reducing the need for frequent hospital visits while alleviating the clinical workload and improving diagnostic efficiency. In addition, small veterinary clinics often face challenges such as low testing volumes and sensitivity to equipment costs, creating a strong demand for affordable, high-performance diagnostic devices. Furthermore, identifying the most likely pathogens responsible for infections is a primary concern for clinical veterinarians. The WeD-1 Pro, a low-cost, IoT-enabled on-site testing system, is well-equipped to address these needs. This system not only supports rapid point-of-care diagnostics but also enables real-time data management and the monitoring of disease and epidemic pathogens through cloud connectivity.

To evaluate the WeD-1 Pro system's performance, we deployed it across 40 small veterinary clinics in China's Greater Bay Area (Fig. S8). Using a 7-plex molecular diagnostic kit for feline respiratory pathogens (provided by Hangzhou EzDx Technology Co., Ltd), we analyzed 1000 tests between December 2024 and September 2025. The results showed that 87% of the cats tested positive for at least one pathogen. *Chlamydia psittaci* (*C. psittaci*) was the most prevalent (73%), followed by Feline calicivirus (FCV, 38%), feline influenza A virus (FIAV, 30%), *Mycoplasma felis* (MF, 22%), feline herpesvirus (FHV, 15%), *Bordetella bronchiseptica* (Bb, 9.8%), and *Chlamydophila felis* (*CF*, 4.7%) (Fig. 6d). Co-infections were common, occurring in 55% of all samples; among these, 82% involved *C. psittaci*, representing 45% of the total samples. We hypothesize that the high co-infection rate associated with *C. psittaci* primarily stems from its ability to disrupt the respiratory and ocular mucosal barriers in cats and to interfere with immune function, thereby creating favorable conditions for secondary pathogen invasion and proliferation. To evaluate diagnostic concordance with a reference method, 60 samples were randomly selected from this field-deployment cohort and compared with conventional PCR. Among these 60 samples, 59 produced concordant results, corresponding to a concordance rate of 98% (59/60). In the single discrepant case, PCR identified both *C. psittaci* and FCV as positive, while the WeD-1 Pro detected only *C. psittaci*. Thus, the 1000-test dataset demonstrates field deployability and real-world

usage, whereas the 60-sample PCR comparison subset provides reference-method validation. Operationally, the WeD-1 Pro system demonstrated outstanding ease of use. Its streamlined workflow—requiring only three steps (sampling, lysis, and direct loading)—substantially reduced hands-on time and workload for clinic staff (Fig. 6a). Moreover, all test results were automatically uploaded to the cloud, enabling data integration for an ongoing pet disease early-warning and surveillance system, and future epidemiological studies.

Usability assessment and user feedback. To systematically evaluate the ease of use and workflow simplification of the WeD-1 Pro system, we conducted usability assessments during field deployment across 40 veterinary clinics. A total of 45 valid structured questionnaires were collected from frontline operators. Statistical analysis based on a 5-point Likert scale showed high ratings for system usability (4.75/5.0), workflow fluency (4.82/5.0), and perceived accuracy and trust (4.68/5.0). In addition, qualitative thematic analysis of open-ended feedback indicated strong user recognition of the AI-guided "zero learning curve", the "error-proof workflow" that helps prevent operational mistakes, and the "documentation relief" provided by automated cloud reporting. Together, these quantitative and qualitative results demonstrate that the WeD-1 Pro system helps reduce the operational barriers of molecular diagnostics and shows strong usability in primary care and non-professional clinical settings. Detailed survey statistics are provided in Table S7.

3.7. Environmental tolerance and field reliability of the WeD-1 Pro system.

To further assess the field reliability of the WeD-1 Pro system, we evaluated device performance under representative conditions, including different ambient temperatures, high humidity, and low-battery or unstable-power conditions (Table S8). The device maintained stable operation across 15 °C to 35 °C and under 76–80% relative humidity, which is typical for Hangzhou. Simulated voltage fluctuation, with the power supply periodically varying between 85% and 110% of the rated voltage, and low-power conditions (30%) were also tested. Under these conditions, the valid-test rate remained above 99%.

We analyzed 1500 on-site tests recorded in the EzDx Cloud during field deployment. The WeD-1 Pro achieved a 98.2% valid-test rate, with most invalid or failed tests attributed to sampling or initial operator loading errors rather than intrinsic device malfunction. These results demonstrate that the WeD-1 Pro maintains reliable performance under varying environmental and power conditions, supporting its use for routine molecular diagnostics in field and primary care settings.

4. Conclusions

The WeD-1 Pro system represents a groundbreaking advancement in molecular POCT for both human and veterinary diagnostics. With its AI-powered assistant and multi-terminal platform, the WeD-1 Pro provides rapid, cost-effective, reliable, and highly sensitive diagnostics, making it an ideal solution for both at-home and primary care applications (see comparison with other molecular detection devices in Table S9). Through systematic screening of polymer substrates and organic optical filter pigments, tailored Pc blue demonstrated superior 480 nm excitation blocking and optimal 525 nm transmission when incorporated into PC, making it suitable for injection-molded focal filter fabrication. By integrating fluorescence detection with injection-molded focal filters, the system overcomes limitations of conventional designs, enhancing sensitivity while maintaining affordability.

In human diagnostics, the WeD-1 Pro has demonstrated exceptional performance in detecting a range of common respiratory pathogens, including SARS-CoV-2 and influenza, with a detection limit as low as 100 copies per reaction. In a proof-of-concept demonstration of at-home self-testing, it showed 100% concordance with results obtained from a commercial qPCR kit using nasal swab samples, further confirming its accuracy and reliability. The AI-based model for automatic result interpretation ensures accurate classification without the need for manual threshold settings, making it user-friendly even for first-time users.

For veterinary diagnostics, the system showed excellent performance in small clinics, where it successfully detected feline respiratory pathogens with a high level of accuracy (98% concordance with PCR results, n = 60). Notably, an overall positivity rate of 87% and a high rate of co-infections were observed.

Overall, the WeD-1 Pro is a transformative tool in the field of molecular diagnostics, providing a practical, scalable, and reliable solution for a wide range of applications. Its ability to deliver precise diagnostics in non-laboratory environments has the potential to revolutionize both individual health management and primary care systems globally. Furthermore, its cloud connectivity capability has important implications for future epidemiological studies and real-time disease surveillance.

Author contributions

Jinzhao Song: conceived the study, designed the experiments, interpreted the data, analyzed the results, and supervised the study. Feibiao Pang: designed the structure and PCB. Tao Zhang: designed the guide and primers and performed the experiments. Yinghao Du: developed the mobile device application and contributed to the development of the AI assistant. Chengen Song: developed the web application and contributed to the development of the AI assistant. Yao Chen: developed the automatic PDF report generation system. All authors contributed to the discussion and reviewed the final manuscript.

Conflicts of interest

Jinzhao Song and Feibiao Pang are co-inventors on three patents related to this work: 1. CN202210983377.8A (filed August 16, 2022); PCT/CN2023/109464 (filed July 27, 2023); CN115404159B (granted April 07, 2026). 2. CN202323212433.7 (filed November 14, 2023); PCT/CN2024/130294 (filed November 06, 2024); CN221797546U (granted October 01, 2024). 3. CN202420282760.5 (filed February 06, 2024); CN222144862U (granted December 10, 2024). The remaining authors declare no competing interests.

Data availability

Supplementary Information (SI), including videos, is provided to give additional details on the device design, operational workflow, functional applications, and experimental results. The SI videos demonstrate the functionality and effectiveness of the WeD-1 Pro system, helping to illustrate the integrated multi-terminal platform and AI-powered assistant for molecular point-of-care testing. The Supplementary Information also includes additional figures and tables covering focal filter design and performance, WeD-1 Pro device and software validation, respiratory pathogen assay data, primer and sgRNA sequences, AI model evaluation, usability and reliability testing, field deployment, and comparisons with other devices. See DOI: https://doi.org/10.1039/d6lc00214e.

Acknowledgements

This study was supported by the National Key Research and Development Program of China (2023YFD2402100) and Zhejiang Leading Innovation and Entrepreneurship Team Program (2022R01006).

References

1 A. A. Adalja, At-home infectious disease testing: An idea whose time has come, *Antimicrob. Steward. Healthc. Epidemiol.*, 2022, **2**(1), e170.
2 F. Dai, *et al.*, A compact, palm-sized isothermal fluorescent diagnostic intelligent IoT device for personal health monitoring and beyond via one-tube/one-step LAMP-CRISPR assay, *Biosens. Bioelectron.*, 2025, **270**, 116945.
3 J. Dinnes, *et al.*, Rapid, point-of-care antigen tests for diagnosis of SARS-CoV-2 infection, *Cochrane Database Syst. Rev.*, 2022, **7**(7), CD013705.
4 E. Dolgin, The future of at-home molecular testing, *Nature*, 2024, DOI: 10.1038/d41586-024-00854-7.
5 K. Wang, *et al.*, Mini-program enabled IoT intelligent molecular diagnostic device for co-detection and spatiotemporal mapping of infectious disease pathogens, *Anal. Chem.*, 2024, **96**(33), 13494–13503.
6 F. Pang, *et al.*, A handheld isothermal fluorescence detector for duplex visualization of aquatic pathogens via enhanced one-pot LAMP-PfAgo assay, *Biosens. Bioelectron.*, 2024, **254**, 116187.
7 J. Song, *et al.*, Single-and two-stage, closed-tube, point-of-care, molecular detection of SARS-CoV-2, *Anal. Chem.*, 2021, **93**(38), 13063–13071.
8 M. Zhang and S. Li, Controllable liquid colour-changing lenses with microfluidic channels for vision protection, camouflage and optical filtering based on soft lithography fabrication, *Springerplus*, 2016, **5**(1), 580.
9 J. A. Dobrowolski, Optical properties of films and coatings, *Handbook of Optics I*, 1995, pp. 42.3–130.
10 T. R. Kozel and A. R. Burnham-Marusich, Point-of-care testing for infectious diseases: past, present, and future, *J. Clin. Microbiol.*, 2017, **55**(8), 2313–2320.
11 J. C. Rolando, A. V. Melkonian and D. R. Walt, The present and future landscapes of molecular diagnostics, *Annu. Rev. Anal. Chem.*, 2024, **17**(1), 459–474.
12 A. Larsson, R. Greig-Pylypczuk and A. Huisman, The state of point-of-care testing: a European perspective, *Upsala J. Med. Sci.*, 2015, **120**(1), 1–10.
13 K. Senthil Kumar, *et al.*, Artificial intelligence in clinical oncology: from data to digital pathology and treatment, *Am. Soc. Clin. Oncol. Educ. Book*, 2023, **43**, e390084.
14 Y. Zu, H. Chang and Z. Cui, Molecular point-of-care testing technologies: current status and challenges, *Nexus*, 2025, **2**(2), 100059.
15 M. L. Cavuto, *et al.*, Portable molecular diagnostic platform for rapid point-of-care detection of mpox and other diseases, *Nat. Commun.*, 2025, **16**(1), 1–13.
16 T. S. Pillay, A. I. Khan and S. Yenice, Artificial intelligence (AI) in point-of-care testing, *Clin. Chim. Acta*, 2025, **574**, 120341.
17 G.-R. Han, *et al.*, Machine learning in point-of-care testing: innovations, challenges, and opportunities, *Nat. Commun.*, 2025, **16**(1), 3165.
18 S. Li, *et al.*, Machine learning-driven multi-emission fluorescence array for simultaneous size discrimination and quantification of gold nanoparticles, *Anal. Chem.*, 2025, **97**(25), 13602–13608.
19 J. Song, *et al.*, Smartphone-based mobile detection platform for molecular diagnostics and spatiotemporal disease mapping, *Anal. Chem.*, 2018, **90**(7), 4823–4831.
20 H. Luo, *et al.*, Highly sensitive and on-site chemosensor for hexavalent chromium detection based on DNA photooxidation cleavage, *Sens. Actuators, B*, 2025, 139057.
21 R. Lu, *et al.*, Field detection of uranyl in coastal water of China using a portable device via DNA photocleavage, *Anal. Chem.*, 2024, **96**(28), 11525–11532.